PLANETARY SCIENCE

The end of the lunar dynamo

Saied Mighani[1]*†, Huapei Wang[1,2]*†, David L. Shuster[3,4], Cauê S. Borlina[1],
Claire I. O. Nichols[1], Benjamin P. Weiss[1]†

Magnetic measurements of the lunar crust and Apollo samples indicate that the Moon generated a dynamo magnetic field lasting from at least 4.2 until <2.5 billion years (Ga) ago. However, it has been unclear when the dynamo ceased. Here, we report paleomagnetic and $^{40}Ar/^{39}Ar$ studies showing that two lunar breccias cooled in a near-zero magnetic field (<0.1 µT) at 0.44 ± 0.01 and 0.91 ± 0.11 Ga ago, respectively. Combined with previous paleointensity estimates, this indicates that the lunar dynamo likely ceased sometime between ~1.92 and ~0.80 Ga ago. The protracted lifetime of the lunar magnetic field indicates that the late dynamo was likely powered by crystallization of the lunar core.

INTRODUCTION

The intensity of the present-day magnetic field across much of the lunar surface is <0.2 nT, indicating that the Moon currently does not have a global magnetic field (1). However, paleomagnetic measurements of Apollo samples indicate that the Moon once generated a core dynamo with surface field intensities of several tens of microtesla (comparable to that of Earth today) during the period 4.25 to 3.56 billion years (Ga) ago (2–7). Following this high-field epoch, the field declined by at least an order of magnitude by 3.2 Ga ago (8) and persisted in a weakened state (~5 µT) until at least 2.5 Ga ago (9). It has been unknown how long the dynamo persisted beyond this time. The youngest lunar paleointensity constraint is an upper limit of 7 µT at <7 million years (Ma) ago provided by an impact glass splash (10).

The time of the dynamo's cessation has major implications for the mechanism of magnetic field generation as well as the thermal and mechanical evolution of the lunar interior (6). For example, a core dynamo powered purely by thermal convection (11–14) is thought to only be able to persist until ~3.5 Ga ago (15). In comparison, a mechanical dynamo driven by mantle precession (16) is thought to be sustainable until sometime between ~3.4 and 2.0 Ga ago for typical lunar physical parameters (6, 9). Alternatively, a thermochemical convection dynamo powered by core crystallization could power the dynamo even until close to the present time (15, 17).

To constrain the late history of the lunar magnetic field, we studied the paleomagnetism of the young Apollo 15 breccias 15465 and 15015 (18). During the assembly of these breccias, their clasts were welded together by 60 to 90 volume % matrix melt glass formed by impact melting of the local lunar regolith (section S1) (19). Breccia 15465 was a float sample collected from the rim of Spur crater and contains clasts with diameters ranging from <1 to ~80 mm that are dominantly regolith breccias (figs. S1 and S7). Our $^{40}Ar/^{39}Ar$, $^{38}Ar/^{36}Ar$, and $^{40}Ar/^{36}Ar$ measurements, combined with previous Ar analyses, indicate that the assembly of 15465 and the formation of its matrix glass most likely occurred at 0.44 ± 0.01 Ga ago (age ranges are 1 SD), while a ~20-mm-diameter regolith breccia clast formed at >3.4 Ga

ago (section S7, table S20, and fig. S38). The latter clast contains a diversity of subclasts, including anorthosites, norites, and KREEP (potassium–rare earth element–phosphorus)–rich basalts that resemble the nearby Apollo 15 basalts (20, 21). Sample 15015 is a regolith breccia collected as float on the mare surface ~20 m from the Apollo 15 Lunar Module (19, 22). It contains <0.1- to 7-mm-diameter clasts in the form of rock, mineral, and glass fragments (figs. S2 and S11). Our $^{40}Ar/^{39}Ar$, $^{38}Ar/^{37}Ar$, and $^{40}Ar/^{36}Ar$ chronometry data indicate that 15015's matrix glass likely formed at 0.91 ± 0.11 Ga ago, consistent with previous measurements (see section S7, table S21, and fig. S39). Combined with our thermal diffusion calculations (section S2), these data indicate that the matrix melt glass, clasts smaller than ~10 mm in diameter, and the thermally equilibrated exteriors of larger clasts should have recorded any ambient lunar magnetic field at ~0.4 Ga ago (15465) and ~0.9 Ga ago (15015).

Similar to previously studied regolith breccias (9), the ferromagnetic carriers in the glassy matrices of 15015 and 15645 have exceptional magnetic recording properties compared to most lunar rocks (section S6). Our electron microscopy observations indicate that the dominant ferromagnetic minerals in the glass matrix of 15465 are kamacite (α-Fe$_{1-x}$Ni$_x$ with x < ~0.04) and schreibersite (Fe$_{1-x}$Ni$_x$)$_3$P with x ~ 0.1, while the aforementioned glassy regolith breccia clast contains mostly kamacite and martensite (α$_2$-Fe$_{1-x}$Ni$_x$ with x ~ 0.08) (fig. S24). Previous analytical electron microscopy (AEM) studies of the matrix glass in 15015 found that it contains kamacite (23), while our electron microscopy observations identified both kamacite and schreibersite (fig. S28). Our hysteresis and isothermal remanent magnetization (IRM) and first-order reversal curve (FORC) measurements of the regolith breccia clast in 15465 and the glass matrix in 15015, along with the AEM data (23), indicate a dominantly single-vortex to superparamagnetic grain size, while the glass matrix in 15465 contains grains ranging from single domain to multidomain in size (figs. S25 to S27, S29, and S30).

Given the mineralogies and compositions of the ferromagnetic grains in 15465 and 15015, these grains should have acquired mostly a total thermoremanent magnetization (TRM) in any ambient magnetic field following the last major heating event (see section S6). The degree of crystallinity in the matrix glasses of the two breccias indicates that they cooled from the 780°C Curie point of kamacite to ambient surface temperatures over >24 hours (section S2 and fig. S4). Because this time scale exceeds the estimated lifetime of putative impact-generated fields from even the largest lunar impacts (24), the matrix glasses in these breccias should have only recorded any ambient dynamo field during cooling. The lack of microfractures in the

[1]Department of Earth, Atmospheric, and Planetary Sciences, Massachusetts Institute of Technology (MIT), 77 Massachusetts Avenue, Cambridge, MA 02139, USA. [2]School of Earth Sciences, China University of Geosciences (Wuhan), 388 Lumo Road, Wuhan, Hubei 430074, P. R. China. [3]Department of Earth and Planetary Science, University of California, Berkeley, Berkeley, CA 94720, USA. [4]Berkeley Geochronology Center, 2455 Ridge Road, Berkeley, CA 94709, USA.
*These authors contributed equally to this work.
†Corresponding author. Email: bpweiss@mit.edu (B.P.W.); huapei@mit.edu (H.W.); smighani@mit.edu (S.M.)

glass matrices of both breccias (see figs. S1 and S2) constrains post-cooling peak shock pressures to below ~3 GPa (25).

We analyzed the paleomagnetism of the breccias in the Massachusetts Institute of Technology (MIT) Paleomagnetism Laboratory using a 2G Enterprises superconducting rock magnetometer (SRM), focusing on the matrix glass. Natural remanent magnetization (NRM) components were determined using alternating field (AF) and thermal demagnetization. Paleointensities were estimated using both nonthermal [i.e., anhysteretic remanent magnetization (ARM) and IRM] and double-heating (26) experiments (sections S3 and S4). To mitigate thermochemical alteration, the thermal demagnetization and paleointensity experiments were conducted in a CO_2-H_2 gas-mixing controlled-atmosphere oven (27) at an oxygen fugacity of 0.5 to 1 log unit below the iron-wüstite buffer (28, 29). We measured the paleomagnetism of 8 and 22 matrix glass–rich subsamples of 15465 and 15015, respectively, 3 subsamples of the regolith breccia clast of 15465, 1 subsample of a ~7-mm-diameter 15015 clast, and 2 composite 15015 subsamples each composed of a single large clast and surrounding matrix glass. Note that the matrix glass–rich subsamples from 15015 also commonly contain some small (<1-mm-diameter) clasts. To our knowledge, the NRM of 15465 has never been previously studied. Two previous studies briefly characterized the IRM (30) of 15015 and estimated paleointensities using nonthermal experiments (31) (section S3).
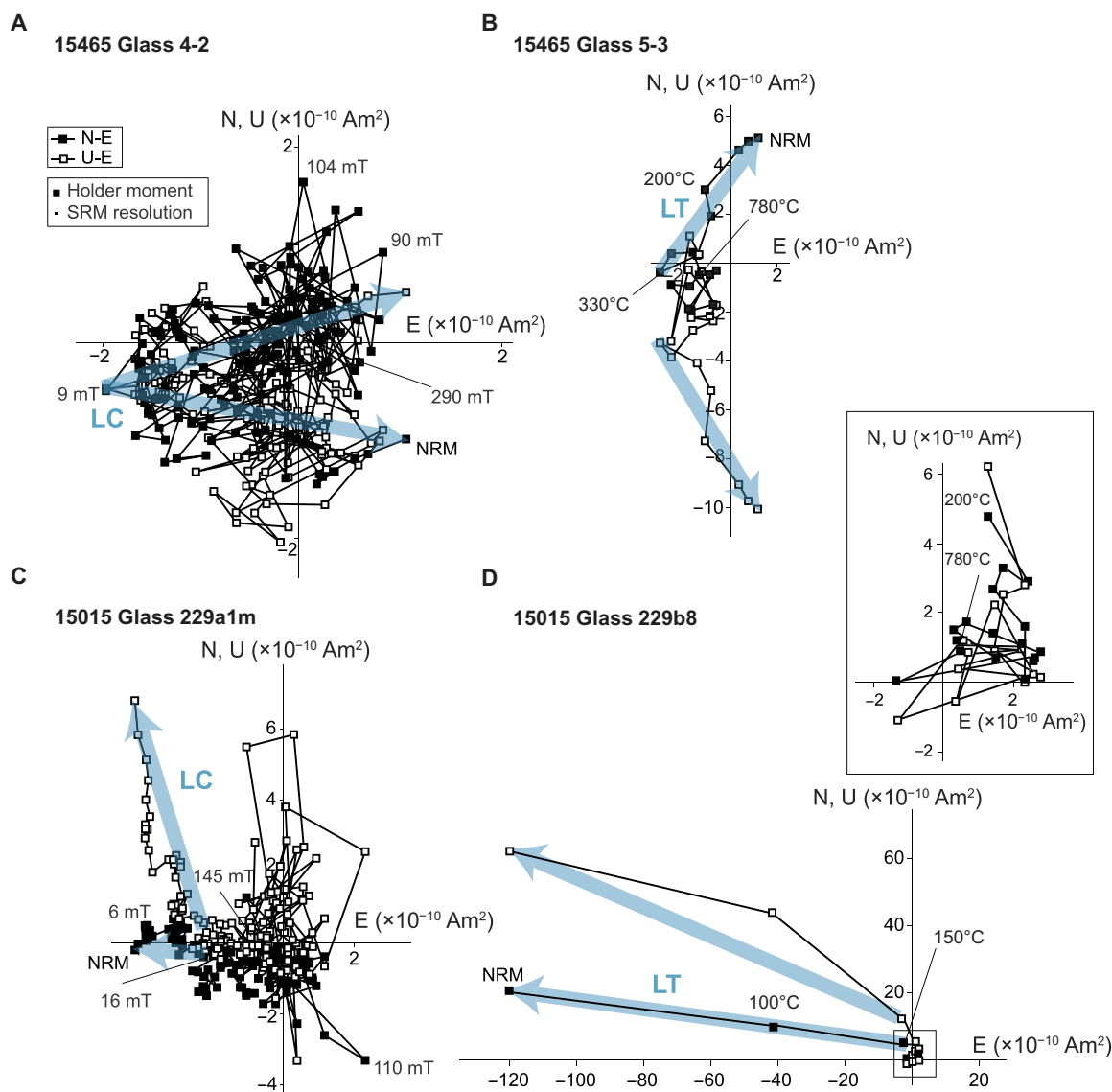

Fig. 1. NRM demagnetization of matrix glass subsamples from breccias 15465 and 15015. Shown are endpoints of the NRM vectors during progressive alternating field (AF) and thermal demagnetization. Closed and open symbols represent projections of the NRM vectors onto the horizontal (N-E) and vertical (U-E) planes, respectively. (**A**) 15465 subsample 4-2. (**B**) 15465 subsample 5-3. (**C**) 15015 subsample 229a1m. (**D**) 15015 subsample 229b8. Inset: Magnified view of HT demagnetization steps for 229b8. The legend in (A) shows the sample holder magnetic moment (denoted by the size of the large black box) and the MIT SRM moment resolution (denoted by the size of the small black box) (section S3). The initial NRM, AF levels, and temperatures for selected demagnetization steps are labeled. For both breccias, after removal of low coercivity (LC) and low temperature (LT) components (blue arrows), there is no discernible origin-trending magnetization in the high coercivity (HC)/high temperature (HT) range (as indicated by scattered vector endpoints).

RESULTS

Breccia 15465

We found that the matrix glass in 15465 contains a low coercivity (LC) and a low temperature (LT) component that unblocked by ~3 to 10 mT and 330° to 390°C, respectively (Fig. 1, fig. S9, and table S4). This component is non-unidirectionally oriented throughout the sample (fig. S8A). Given that the matrix glass was heated above the kamacite Curie temperature during its formation and so should have acquired a stable, unidirectional magnetization in the direction of any ambient field, the low AF and thermal stability and the non-unidirectionality of these components suggest that they are secondary

and postdate breccia formation. Blocking temperature relationships for single-domain and single-vortex iron indicate that lunar samples are expected to have viscous overprints with 1-hour blocking temperatures somewhere between ~125° and 485°C (32, 33), consistent with the observed peak unblocking temperature of the LC component. Our laboratory viscous remanent magnetization (VRM) experiments indicate that the magnitude of terrestrial VRM acquired over four decades of storage in Earth's magnetic field at Johnson Space Center (JSC) could have reached ~130% of the LC/LT components (section S5). Therefore, the LC/LT components are likely VRMs acquired in the geomagnetic field, although there may also
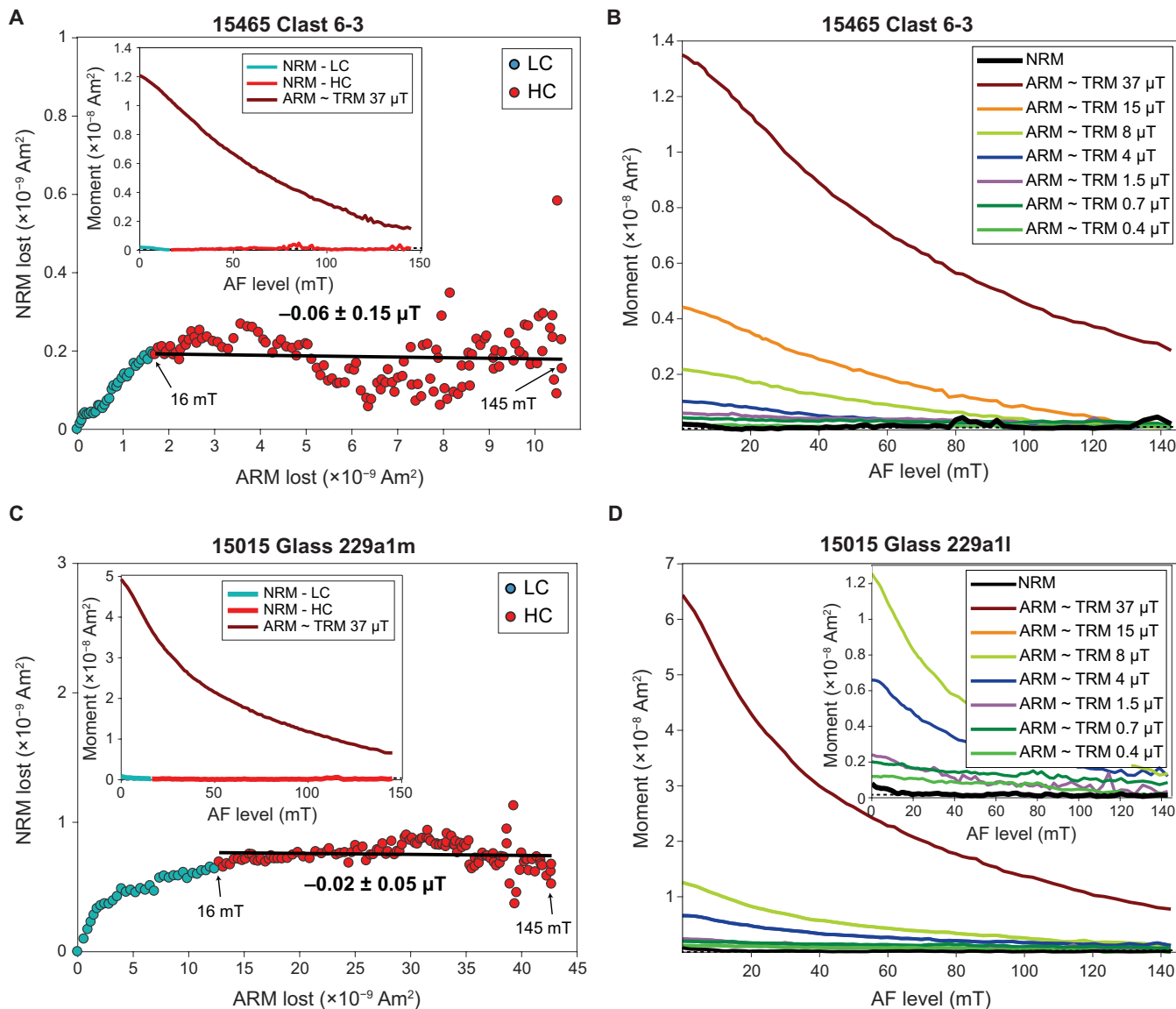

Fig. 2. Paleointensity estimates for subsamples of breccias 15465 and 15015. (**A** and **C**) ARM paleointensity experiments on 15465 subsample 6-3 and 15015 subsample 229a1m, respectively. Paleointensities are estimated from NRM lost during AF demagnetization as a function of ARM gained in a 50-μT DC bias field and a 260-mT AF. AF steps used to calculate the LC and HC paleointensities are colored blue and red, respectively. Paleointensities and their uncertainties (95% confidence intervals) are shown for the HC range. Insets in (A) and (C) show the decay of NRM and ARM during progressive AF demagnetization. (**B** and **D**) ARM paleointensity fidelity tests on 15465 subsample 6-3 and 15015 subsample 229a1l, respectively. Legends list TRM-equivalent fields for ARMs acquired in a range of DC bias fields in an AF of 260 mT and assuming ARM/TRM = 1.34 (section S4) (49). Horizontal dashed lines indicate the noise level due to acquisition of spurious ARM during AF demagnetization. Inset in (D) shows a magnified view of the moment decay.

be a contribution from exposure to stray fields during handling by the astronauts or at JSC (*34*). The LC/LT components for the clast subsamples unblocked by ~16 to 65 mT (fig. S9) and 200°C (fig. S10B) and likely have similar origins to those in the matrix glass (section S3).

After removal of the LC/LT components in 15465, further demagnetization of matrix glass samples produced directionally unstable moments with no consistent decay in magnitude (Fig. 1 and fig. S9). Principal components analysis (PCA) of these high coercivity (HC) and high temperature (HT) ranges yielded non–origin-trending components [deviation angle > maximum angular deviation (MAD) (*35*); table S4] with highly scattered directions and most MAD values >40° (fig. S8B and table S4). This indicates the absence of any HC/HT components and a lack of total TRM in the glass subsamples. Furthermore, we found that the ARM, IRM, and thermal paleointensities for the glass subsamples are within error of zero for the HC/HT range (Fig. 2, figs. S16 and S18, tables S6 to S7, and section S4). For the nonthermal paleointensities, the mean HC paleointensity value for glass samples is $-0.10 \pm 0.08\,\mu$T (paleointensity ranges are 2 SDs), with ~90% of experiments yielding nominal values of <0.7 μT. Glass sample HT thermal paleointensities are less well constrained but also near zero (mean value of $3.8 \pm 2.9\,\mu$T). Partial TRM (pTRM) checks during the thermal experiments indicate a lack of thermochemical alteration during laboratory heating up to 730°C (section S4 and fig. S18), although the samples acquired substantial pTRM during in-field heating steps. Like the matrix glass samples, we also found that subsample 6-3, which is from the exterior of the 15465 regolith breccia clast that is expected to have been heated above the kamacite Curie temperature by surrounding matrix melt after breccia assembly, exhibits an unmagnetized HC range (ARM and IRM mean paleointensity of $-0.13 \pm 0.22\,\mu$T and residual ARM paleointensity of <0.06 μT) (Fig. 2A, tables S6 and S7, and section S4). The lack of stable NRM in 15465 is not only due to poor magnetic recording properties of the sample: Our 15465 paleointensity fidelity analyses indicate that our nonthermal methods can accurately measure paleointensities of <0.4 μT (Fig. 2B, section S4, and table S11). Overall, our measurements of 15465 show that the lunar surface field was almost certainly below 0.4 μT and very likely below even 0.06 μT, at the time it was assembled at 0.44 ± 0.01 Ga ago.

Breccia 15015

Demagnetization of 15015 glass-rich, clast, and composite clast glass subsamples yielded similar results. Subsamples taken from within 2.7 mm of two surfaces previously cut with a bandsaw at JSC in 1971 have NRM intensities and directions that correlate with the position of the subsamples (fig. S15D, table S5, and section S3). Subsamples with surfaces cut by the JSC bandsaw have stable, origin-trending LC/LT components with low unblocking temperatures (150°C) (Fig. 1D) but high peak coercivities (>145 mT) (fig. S13, C and D). The LC/LT components are collectively highly non-unidirectional but have directions dispersed approximately along a great circle and correlated with the distance of the subsamples from the two JSC sawcut surfaces (fig. S15C). The peak AF levels and unblocking temperatures of the LC/LT components also correlate with distance from the JSC sawcuts (fig. S15 and table S5). These LC/LT components have a paleointensity of ~5 to 69 μT, within the range of Earth's present surface field (table S8 and section S4). These observations indicate that the LC/LT overprints are likely overprints acquired during bandsaw cutting at JSC, which has been shown to partially thermally remagnetize sam-

ples due to the lack of a coolant (*8*). By comparison, for glass subsamples located >3.4 mm from either JSC sawcut, the LC/LT components unblocked by just ~2 to 16 mT and <150°C (Fig. 1C; fig. S13, A and B; and table S5). The low AF and thermal stability and non-unidirectionality of these components (fig. S12) suggest that they are also recent overprints. Our laboratory VRM acquisition experiments indicate that the magnitudes of the LC/LT components of these interior samples are consistent with their origin as a terrestrial VRM (section S5) with a possible weak contribution from bandsaw heating.

As with the 15465 subsamples, after removal of the LC/LT components, we found that the remaining NRM does not consistently weaken in intensity or maintain a stable orientation during further demagnetization in the HC/HT range (Fig. 1, C and D, and fig. S13), with PCA fits yielding scattered, non–origin-trending fits with MAD values >30°. As with 15465, this again indicates the absence of an HC/HT component. Our HC/HT ARM and IRM paleointensities (Fig. 2C, fig. S17, and tables S7 and S8) are indistinguishable from zero (with glass samples having a mean value of $-0.01 \pm 0.02\,\mu$T and 68% of samples having nominal values of <0.1 μT) and the residual ARM paleointensity of <0.08 μT. Our thermal paleointensity experiments measured an HT mean value of $0.31 \pm 0.18\,\mu$T (Fig. 3, fig. S19, and table S8), with pTRM checks (table S10) demonstrating that no substantial thermochemical alteration occurred up to 680°C. Our paleointensity fidelity measurements indicate that 15015 can accurately record paleofields of <0.7 μT (Fig. 2D and section S4). Collectively, these data indicate a lack of total TRM during the breccia formation. We conclude that the matrix glass of breccia 15015 certainly formed in a field of no more than 0.7 μT and very likely less than 0.08 μT at 0.91 ± 0.11 Ga ago.

DISCUSSION
Our results from both breccias show that the lunar surface field was very likely below 0.06 and 0.08 μT at 0.44 ± 0.01 Ga ago and 0.91 ± 0.11 Ga ago, respectively. These upper limits are at or below inferred lunar
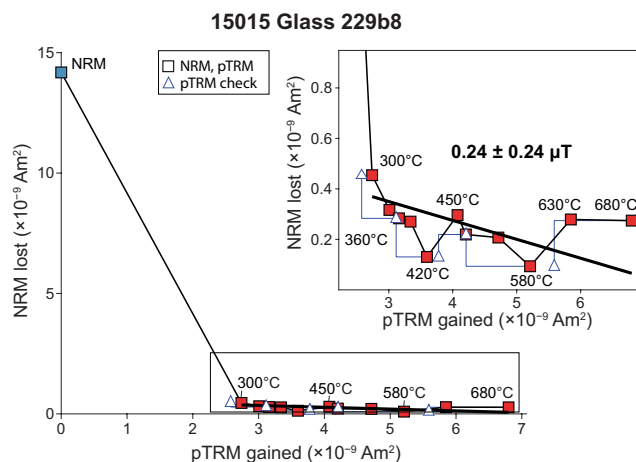

Fig. 3. Thermal paleointensity estimate for 15015 matrix glass. Shown is the NRM lost during progressive thermal demagnetization versus pTRM gained by heating in a laboratory field of 3 μT for subsample 229b8. Inset: Magnified view of 300° to 680°C temperature steps. NRM lost and pTRM gained steps are denoted with squares, with blue and red symbols denoting data in the LT and HT ranges, respectively. pTRM checks for alteration are denoted with triangles. The HT range has a paleointensity value of 0.24 ± 0.24 μT.
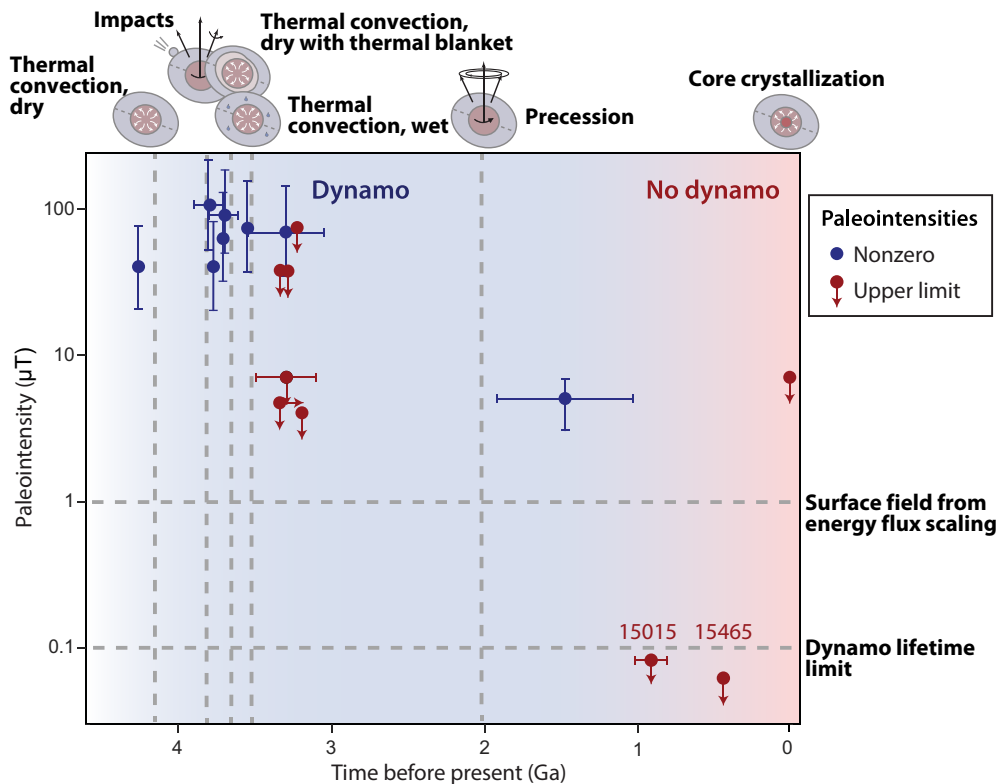
Fig. 4. Paleointensities for breccias 15465 and 15015 and those of other modern measurements of lunar rocks. Points labeled 15015 and 15465 are new paleointensity estimates reported by this study, while the remaining points are previously measured values (*6*, *9*). Red points denote upper limits on the field (i.e., values indistinguishable from zero), while blue points denote nonzero values (i.e., detections of the paleofield). Vertical and horizontal arrows and error bars indicate the paleointensity and age limits and 1-SD uncertainties, respectively. The blue and red shaded regions indicate the epochs when the dynamo is inferred to be active and have ceased, respectively. Vertical and horizontal arrows and error bars indicate the paleointensity and age limits and uncertainties, respectively. The vertical dashed lines are the lifetime for proposed dynamo mechanisms: thermal convection in a dry mantle (*11*), impact-driven changes in mantle rotation (*50*), thermal convection in a dry mantle covered by a thermal blanket (*12*), thermal convection in a wet mantle (*13*), lunar precession (*16*), and core crystallization (*15*). The upper and lower horizontal dashed lines denote the maximum field predicted by energy flux scaling (*36*) and the predicted field exceeded by all published dynamo models for >90% of the dynamo lifetime, respectively. Data are tabulated in table S22.

surface fields over much of the mare (*1*) and compatible with the weak fields measured at the Apollo 15 site (*2*). These upper limits are also below the surface fields typically predicted by dynamo scaling laws (*36*): In particular, all published lunar thermal and evolution models (*12*, *14*–*16*, *37*, *38*) predict surface fields of >0.1 μT for >~90% of the dynamo's active period. Such a weak intensity is also below the weakest known dynamo surface field in the solar system today, that of Mercury (*39*). Therefore, we conclude that the lunar dynamo was likely no longer operating at 0.91 ± 0.11 Ga ago.

The youngest evidence for the existence of the lunar dynamo is the ~5 ± 2 μT paleointensity estimate from regolith breccia 15498, whose age of assembly is constrained using $^{40}Ar/^{39}Ar$ chronometry (*9*) to ~1.75 ± 0.75 Ga ago and using trapped $^{40}Ar/^{36}Ar$ data (*40*) to $1.32^{+0.59}_{-0.52}$ (section S7.5). We obtain a new refined age of the NRM in 15498 by adopting the weighted mean of these two ages of 1.47 ± 0.45 Ga ago. Combining the 1-SD extremes of the age estimates for 15498 and 15015, we conclude that the dynamo ceased sometime between 1.92 and 0.80 Ga ago. Furthermore, the age and paleointensity constraints on 15465 indicate that the dynamo field remained absent at 0.44 ± 0.01 Ga ago (Fig. 4). Such a protracted history is likely inconsistent with the late magnetic field being generated by precession (*16*, *41*), which is thought to have only been capable of powering a dynamo until

~2.0 Ga ago given the expected evolution of the lunar orbit (*9*). Instead, the persistence of the magnetic field until after 1.92 Ga ago is likely compatible with the late dynamo being driven by core crystallization for relatively low values of core thermal conductivity and expansivity (*17*). Future paleointensity studies on young Apollo samples should determine whether the dynamo ceased permanently after 1.92 Ga ago or, alternatively, whether it entered a start-stop regime (*17*).

METHODS
Paleomagnetism
Paleomagnetic analyses were conducted using a 2G Enterprises SRM 755 inside the MIT Paleomagnetism Laboratory. We prepared mutually oriented subsamples of 15465 and 15015 in this shielded room using a wire saw previously shown to not measurably disturb the NRM of lunar samples (*8*).

Static three-axis AF demagnetization of NRM was conducted up to a maximum AF of 145 mT for most subsamples (in some cases, up to 290 mT). Thermal demagnetization and thermal paleointensity experiments were conducted up to 780°C in a CO_2-H_2 gas-mixing controlled-atmosphere oven (*27*) at an oxygen fugacity set to the estimated formation conditions of lunar materials (0.5 to 1 log units

below the iron-wüstite buffer) (28, 29). ARM and IRM paleointensities were conducted using multicomponent methods (42, 43). The thermal paleointensities were conducted following the IZZI (in-field, zero-field, zero-field, in-field) protocol (44) and included pTRM checks for alteration. NRM components were estimated using PCA (45).

ARM and IRM measurements were obtained using the MIT SRM. Hysteresis and FORC measurements were conducted at the MIT Department of Materials Science and Engineering using a vibrating sample magnetometer.

$^{40}Ar/^{39}Ar$, $^{38}Ar/^{37}Ar$, and $^{40}Ar/^{36}Ar$ chronometry

$^{40}Ar/^{39}Ar$, $^{38}Ar/^{37}Ar$, and $^{40}Ar/^{36}Ar$ thermochronometry experiments were conducted at the Berkeley Geochronology Center following our previously described procedures (4, 8, 46). We analyzed both whole rock matrix glass and clast subsamples from both lithologies. We calculated apparent $^{40}Ar/^{39}Ar$ ages for each degassing step relative to the Hb3gr fluence monitor [age = 1081 Ma (47)] using the decay constants of (47) and the isotopic abundances of (48). For 15465 glass subsample 6-4-1, 15465 clast subsample 6-2, and 15015 glass subsample 229b1, we corrected the $^{40}Ar/^{39}Ar$ ages for the trapped ^{40}Ar using the ordinate-intercept $^{40}Ar/^{36}Ar$ ratios determined by error-weighted linear regressions in three-isotope plots. Cosmogenic ^{38}Ar exposure ages for each degassing step were estimated following the procedures described in (46).

SUPPLEMENTARY MATERIALS

REFERENCES AND NOTES

1. D. S. Mitchell, J. S. Halekas, R. P. Lin, S. Frey, L. L. Hood, M. H. Acuña, A. Binder, Global mapping of lunar crustal magnetic fields by Lunar Prospector. *Icarus* **194**, 401–409 (2008).
2. M. Fuller, S. M. Cisowski, Lunar paleomagnetism, in *Geomagnetism*, J. A. Jacobs, Ed. (Academic Press, 1987), vol. 2, pp. 307–455.
3. I. Garrick-Bethell, B. P. Weiss, D. L. Shuster, J. Buz, Early lunar magnetism. *Science* **323**, 356–359 (2009).
4. E. K. Shea, B. P. Weiss, W. S. Cassata, D. L. Shuster, S. M. Tikoo, J. Gattacceca, T. L. Grove, M. D. Fuller, A long-lived lunar core dynamo. *Science* **335**, 453–456 (2012).
5. C. Cournède, J. Gattacceca, P. Rochette, Magnetic study of large Apollo samples: Possible evidence for an ancient centered dipolar field on the Moon. *Earth Planet. Sci. Lett.* **331–332**, 31–42 (2012).
6. B. P. Weiss, S. M. Tikoo, The lunar dynamo. *Science* **346**, 1246753 (2014).
7. I. Garrick-Bethell, B. P. Weiss, D. L. Shuster, S. M. Tikoo, M. M. Tremblay, Further evidence for early lunar magnetism from troctolite 76535. *J. Geophys. Res.* **121**, 76–93 (2017).
8. S. M. Tikoo, B. P. Weiss, W. S. Cassata, D. L. Shuster, J. Gattacceca, E. A. Lima, C. Suavet, F. Nimmo, M. D. Fuller, Decline of the lunar core dynamo. *Earth Planet. Sci. Lett.* **404**, 89–97 (2014).
9. S. M. Tikoo, B. P. Weiss, D. L. Shuster, C. Suavet, H. Wang, T. L. Grove, A two-billion-year history for the lunar dynamo. *Sci. Adv.* **3**, e1700207 (2017).
10. J. Buz, B. P. Weiss, S. M. Tikoo, D. L. Shuster, J. Gattacceca, T. L. Grove, Magnetism of a very young lunar glass. *J. Geophys. Res.* **120**, 1720–1735 (2015).
11. W. Konrad, T. Spohn, Thermal history of the Moon: Implications for an early core dynamo and post-accertional magmatism. *Adv. Space Res.* **19**, 1511–1521 (1997).
12. D. R. Stegman, A. M. Jellinek, S. A. Zatman, J. R. Baumgardner, M. A. Richards, An early lunar core dynamo driven by thermochemical mantle convection. *Nature* **421**, 143–146 (2003).
13. A. J. Evans, M. T. Zuber, B. P. Weiss, S. M. Tikoo, A wet, heterogeneous lunar interior: Lower mantle and core dynamo evolution. *J. Geophys. Res.* **119**, 1061–1077 (2014).
14. F. Takahashi, H. Tsunakawa, Thermal core-mantle coupling in an early lunar dynamo: Implications for a global magnetic field and magnetosphere of the early Moon. *Geophys. Res. Lett.* **36**, L24202 (2009).
15. M. Laneuville, M. A. Wieczorek, D. Breuer, J. Aubert, G. Morard, T. Rückriemen, A long-lived lunar dynamo powered by core crystallization. *Earth Planet. Sci. Lett.* **401**, 251–260 (2014).

16. C. A. Dwyer, D. J. Stevenson, F. Nimmo, A long-lived lunar dynamo driven by continuous mechanical stirring. *Nature* **479**, 212–214 (2011).

17. A. Scheinberg, K. M. Soderlund, G. Schubert, Magnetic field generation in the lunar core: The role of inner core growth. *Icarus* **254**, 62–71 (2015).

18. H. Wang, S. Mighani, B. P. Weiss, D. L. Shuster, K. V. Hodges, Lifetime of the lunar dynamo constrained by young Apollo returned breccias 15015 and 15465. *Proc. Lunar Planet. Sci. Conf.* **48**, 1439 (2017).

19. C. Meyer, *The Lunar Sample Compendium* (2016); https://curator.jsc.nasa.gov/lunar/lsc/index.cfm.

20. S. Simon, J. Papike, D. Gosselin, J. Laul, Petrology, chemistry and origin of Apollo 15 regolith breccias. *Geochim. Cosmochim. Acta* **50**, 2675–2691 (1986).

21. K. Cameron, J. Delano, Petrology of Apollo 15 consortium breccia 15465. *Proc. Lunar Sci. Conf. 4th* **1**, 461–466 (1973).

22. D. S. McKay, D. D. Bogard, R. v. Morris, R. L. Korotev, S. J. Wentworth, P. Johnson, Apollo 15 regolith breccias: Window to a KREEP regolith, in *19th Proceedings of Lunar and Planetary Science Conference* (1989), pp. 19–41.

23. S. Mehta, J. I. Goldstein, Analytical electron microscopy study of submicroscopic metal particles in glassy constituents of lunar breccias 15015 and 60095, in *10th Proceedings of Lunar and Planetary Science Conference* (1979), pp. 1507–1521.

24. L. L. Hood, N. A. Artemieva, Antipodal effects of lunar basin-forming impacts: Initial 3D simulations and comparisons with observations. *Icarus* **193**, 485–502 (2008).

25. S. M. Tikoo, B. P. Weiss, J. Buz, E. A. Lima, E. K. Shea, G. Melo, T. L. Grove, Magnetic fidelity of lunar samples and implications for an ancient core dynamo. *Earth Planet. Sci. Lett.* **337–338**, 93–103 (2012).

26. E. Thellier, O. Thellier, Sur l'intensité du champ magnétique terrestre dans le passé historique et géologique. *Ann. Geophys.* **15**, 285–376 (1959).

27. C. Suavet, B. P. Weiss, T. L. Grove, Controlled-atmosphere thermal demagnetization and paleointensity analyses of extraterrestrial rocks. *Geochem. Geophys. Geosyst.* **15**, 2733–2743 (2014).

28. M. Sato, N. L. Hickling, J. E. McLane, Oxygen fugacity values of Apollo 12, 14, and 15 lunar samples and reduced state of lunar magmas. *Proc. Lunar Planet. Sci. Conf. 4th* **1**, 1061–1079 (1973).

29. H. Mao, A. El Goresy, P. Bell, Evidence of extensive chemical reduction in lunar regolith samples from the Apollo 17 site. *Proc. Lunar Planet. Sci. Conf. 5th* **1**, 673–683 (1974).

30. S. M. Cisowski, D. W. Collinson, S. K. Runcorn, A. Stephenson, M. Fuller, A review of lunar paleointensity data and implications for origin of lunar magnetism. *Proc. Lunar Planet. Sci. Conf. 13th* **88**, A691–A704 (1983).

31. D. W. Collinson, On the existence of magnetic fields on the Moon between 3.6 Ga ago and the present. *Phys. Earth Planet. Inter.* **34**, 102–116 (1984).

32. L. Nagy, W. Williams, L. Tauxe, A. R. Muxworthy, I. Ferreira, Thermomagnetic recording fidelity of nanometer-sized iron and implications for planetary magnetism. *Proc. Natl. Acad. Sci. U.S.A.* **116**, 1984–1991 (2019).

33. I. Garrick-Bethell, B. P. Weiss, Kamacite blocking temperatures and applications to lunar magnetism. *Earth Planet. Sci. Lett.* **294**, 1–7 (2010).

34. G. W. Pearce, W. A. Gose, D. W. Strangway, Magnetic studies on Apollo 15 and 16 lunar samples. *Proc. Lunar Sci. Conf.* **4**, 3045–3076 (1973).

35. K. Lawrence, C. Johnson, L. Tauxe, J. Gee, Lunar paleointensity measurements: Implications for lunar magnetic evolution. *Phys. Earth Planet. Inter.* **168**, 71–87 (2008).

36. U. R. Christensen, Dynamo scaling laws and applications to the planets. *Space Sci. Rev.* **152**, 565–590 (2010).

37. M. Laneuville, M. A. Wieczorek, D. Breuer, N. Tosi, Asymmetric thermal evolution of the Moon. *J. Geophys. Res.* **118**, 1435–1452 (2013).

38. M. Le Bars, M. A. Wieczorek, Ö. Karatekin, D. Cébron, M. Laneuville, An impact-driven dynamo for the early Moon. *Nature* **479**, 215–218 (2011).

39. B. J. Anderson, M. H. Acuña, K. Korth, J. A. Slavin, H. Uno, C. L. Johnson, M. E. Purucker, S. C. Solomon, J. M. Raines, T. H. Zurbuchen, G. Gloeckler, R. L. McNutt Jr., The magnetic field of Mercury. *Space Sci. Rev.* **152**, 307–339 (2010).

40. A. L. Fagan, K. H. Joy, D. D. Bogard, D. A. Kring, Ages of globally distributed lunar paleoregoliths and soils from 3.9 Ga to the present. *Earth Moon Planets* **112**, 59–71 (2014).

41. J. Meyer, J. Wisdom, Precession of the lunar core. *Icarus* **211**, 921–924 (2011).

42. A. Stephenson, D. W. Collinson, Lunar magnetic field palaeointensities determined by an anhysteretic remanent magnetization method. *Earth Planet. Sci. Lett.* **23**, 220–228 (1974).

43. J. Gattacceca, P. Rochette, Toward a robust normalized magnetic paleointensity method applied to meteorites. *Earth Planet. Sci. Lett.* **227**, 377–393 (2004).

44. E. Ben-Yosef, H. Ron, L. Tauxe, A. Agnon, A. Genevey, T. E. Levy, U. Avner, M. Najjar, Application of copper slag in geomagnetic archaeointensity research. *J. Geophys. Res.* **113**, B08101 (2008).

45. J. L. Kirschvink, The least-squares line and plane and the analysis of palaeomagnetic data. *Geophys. J. Int.* **62**, 699–718 (1980).

46. D. L. Shuster, W. S. Cassata, Paleotemperatures at the lunar surfaces from open system behavior of cosmogenic ^{38}Ar and radiogenic ^{40}Ar. *Geochim. Cosmochim. Acta* **155**, 154–171 (2015).

47. P. R. Renne, G. Balco, K. R. Ludwig, R. Mundil, K. Min, Response to the comment by W. H. Schwarz et al. on "Joint determination of ^{40}K decay constants and ^{40}Ar*/^{40}K for the Fish Canyon sanidine standard, and improved accuracy for ^{40}Ar/^{39}Ar geochronology" by P.R. Renne et al. (2010). *Geochim. Cosmochim. Acta* **75**, 5097–5100 (2011).

48. P. R. Renne, C. C. Swisher, A. L. Deino, D. B. Karner, T. L. Owens, D. J. De Paolo, Intercalibration of standards, absolute ages and uncertainties in ^{40}Ar/^{39}Ar dating. *Chem. Geol.* **145**, 117–152 (1998).

49. D. W. Collinson, A. Stephenson, S. K. Runcorn, Magnetic studies of Apollo 15 and 16 rocks. *Proc. Lunar Sci. Conf.* **4**, 2963–2976 (1973).

50. C. Suavet, B. P. Weiss, W. S. Cassata, D. L. Shuster, J. Gattacceca, L. Chan, I. Garrick-Bethell, J. W. Head, T. L. Grove, M. D. Fuller, Persistence and origin of the lunar core dynamo. *Proc. Natl. Acad. Sci. U.S.A.* **110**, 8453–8458 (2013).

51. G. A. Swann, N. C. Bailey, R. M. Baston, V. L. Freeman, M. H. Hait, J. W. Head, H. E. Holt, K. A. Howard, J. B. Irwin, K. B. Larson, W. R. Muehlberger, V. S. Reed, J. J. Rennilson, G. G. Schaber, D. R. Scott, L. T. Silver, R. L. Sutton, G. E. Ulrich, H. G. Wilshire, E. W. Wolfe, in *Apollo 15 Preliminary Science Report* (NASA publication SP-289, 1972), pp. 5.1–5.112.

52. G. Ryder, in *Catalog of Apollo 15 Rocks, Part 2* (NASA Curatorial Branch Publication 72, 1985).

53. The Apollo 15 Preliminary Examination Team, The Apollo 15 lunar samples: A preliminary description. *Science* **175**, 363–375 (1972).

54. T. Plieninger, O. A. Schaeffer, Laser probe ^{39}Ar–^{40}Ar ages of individual mineral grains in lunar basalt 15607 and lunar breccia 15465. *Proc. Lunar Sci. Conf. 7th* **2**, 2055–2066 (1976).

55. R. Schaal, F. Hörz, T. D. Thompson, J. Bauer, Shock metamorphism of granulated lunar basalt. *Proc. Lunar Sci. Conf. 10th*, 2547–2571 (1979).

56. G. Ryder, in *Catalog of Apollo 15 Rocks* (NASA Curatorial Branch Publication 72, 1985), p. 1296.

57. The European Consortium, in *Lunar Sample Studies* (1977), pp. 1–33.

58. J. C. Russ, R. T. Dehoff, *Practical Stereology* (Springer, ed. 2, 2000).

59. D. R. Uhlmann, L. C. Kleine, Crystallization kinetics, viscous flow, and thermal histories of lunar breccias 15286 and 15498. *Proc. Lunar Sci. Conf. 7th*, 2529–2541 (1976).

60. D. S. Mckay, D. A. Morrison, Lunar breccias. *J. Geophys. Res.* **76**, 5658–5669 (1971).

61. J. M. Christie, D. T. Griggs, Electron petrography of Apollo 14 and 15 breccias and shock-produced analogs. *Proc. Lunar Sci. Conf.* **4**, 365–382 (1973).

62. S. W. Kieffer, From regolith to rock by shock. *Moon* **13**, 301–320 (1975).

63. D. Stöffler, H.-D. Knöll, U. Maerz, Terrestrial and lunar impact breccias and the classification of lunar highland rocks. *Proc. Lunar Planet. Sci. Conf. 10th* **1**, 639–675 (1979).

64. J. G. Spray, Lithification mechanisms for planetary regoliths: The glue that binds. *Annu. Rev. Earth Planet. Sci.* **44**, 139–174 (2016).

65. D. R. Uhlmann, L. Klein, R. W. Hopper, Sintering, crystallization, and breccia formation. *Moon* **13**, 277–284 (1975).

66. R. K. Cardwell, D. S. Chinn, G. F. Moore, D. L. Turcotte, Frictional heating on a fault zone with finite thickness. *Geophys. J. Int.* **52**, 525–530 (1978).

67. H. S. Carslaw, J. C. Jaeger, *The Conduction of Heat in Solids* (Oxford Univ. Press, ed. 2, 1959).

68. H. Wang, B. P. Weiss, X. N. Bai, B. G. Downey, J. Wang, J. Wang, C. Suavet, R. R. Fu, M. E. Zucolotto, Lifetime of the solar nebula constrained by meteorite paleomagnetism. *Science* **355**, 623–627 (2017).

69. B. P. Weiss, J. Gattacceca, S. Stanley, P. Rochette, U. R. Christensen, Paleomagnetic records of meteorites and early planetesimal differentiation. *Space Sci. Rev.* **152**, 341–390 (2010).

70. A. Stephenson, Three-axis static alternating field demagnetization of rocks and the identification of natural remanent magnetization, gyroremanent magnetization, and anisotropy. *J. Geophys. Res.* **98**, 373–381 (1993).

71. J. R. Taylor, *An Introduction to Error Analysis: The Study of Uncertainties in Physical Measurements* (University of Science Books, 1997).

72. L. Tauxe, H. Staudigel, Strength of the geomagnetic field in the Cretaceous Normal Superchron: New data from submarine basaltic glass of the Troodos Ophiolite. *Geochem. Geophys. Geosyst.* **5**, Q02H06 (2004).

73. G. Kletetschka, M. A. Wieczorek, Fundamental relations of mineral specific magnetic carriers for paleointensity determination. *Phys. Earth Planet. Inter.* **272**, 44–49 (2017).

74. G. Acton, Q.-Z. Yin, K. L. Verosub, L. Jovane, A. Roth, B. Jacobsen, D. S. Ebel, Micromagnetic coercivity distributions and interactions in chondrules with implications for paleointensities of the early solar system. *J. Geophys. Res.* **112**, B03S90 (2007).

75. Y. Yu, Paleointensity determination using anhysteretic remanence and saturation isothermal remanence. *Geochem. Geophys. Geosyst.* **11**, Q02Z12 (2010).

76. Y. Yu, L. Tauxe, J. S. Gee, A linear field dependence of thermoremanence in low magnetic fields. *Phys. Earth Planet. Int.* **162**, 244–248 (2007).

77. S.-C. L. L. Lappe, J. M. Feinberg, A. R. Muxworthy, R. J. Harrison, Comparison and calibration of nonheating paleointensity methods: A case study using dusty olivine. *Geochem. Geophys. Geosyst.* **14**, 2143–2158 (2013).

78. S. L. Halgedahl, S. R. Day, M. Fuller, The effect of cooling rate on the intensity of weak-field TRM in single-domain magnetite. *J. Geophys. Res.* **95**, 3690–3698 (1980).

79. L. Tauxe, *Essentials of Paleomagnetism: Fifth Web Edition* (2018).

80. G. A. Paterson, L. Tauxe, A. J. Biggin, R. Shaar, L. C. Jonestrask, On improving the selection of Thellier-type paleointensity data. *Geochem. Geophys. Geosyst.* **15**, 1180–1192 (2014).

81. J. F. J. Bryson, B. P. Weiss, R. J. Harrison, J. Herrero-Albillos, F. Kronast, Paleomagnetic evidence for dynamo activity driven by inward crystallisation of a metallic asteroid. *Earth Planet. Sci. Lett.* **472**, 152–163 (2017).

82. D. J. Dunlop, Theory and application of the Day plot (M_{rs}/M_s versus H_{cr}/H_c)—1. Theoretical curves and tests using titanomagnetite data. *J. Geophys. Res.* **107**, EPM 4-1–EPM 4-22 (2002).

83. D. J. Dunlop, Theory and application of the Day plot (M_{rs}/M_s versus H_{cr}/H_c)—2. Application to data for rocks, sediments, and soils. *J. Geophys. Res.* **107**, EPM 5-1–EPM 5-15 (2002).

84. R. J. Harrison, J. M. Feinberg, FORCinel: An improved algorithm for calculating first-order reversal curve distributions using locally weighted regression smoothing. *Geochem. Geophys. Geosyst.* **9**, Q01056 (2008).

85. L. J. Swartzendruber, V. P. Itkin, C. B. Alcock, The Fe-Ni (iron-nickel) system. *J. Phase Equilib.* **12**, 288–312 (1991).

86. J. I. Goldstein, H. Yakowitz, Metallic inclusions and metal particles in the Apollo 12 lunar soil. *Proc. Lunar Sci. Conf.* **2**, 177–191 (1971).

87. A. El Goresy, P. Ramdohr, L. A. Taylor, The geochemistry of the opaque minerals in Apollo 14 crystalline rocks. *Earth Planet. Sci. Lett.* **13**, 121–129 (1971).

88. A. S. Doan, J. I. Goldstein, The ternary phase diagram, Fe-Ni-P. *Metall. Trans.* **1**, 1759–1767 (1970).

89. R. J. Gambino, T. R. McGuire, Y. Nakamura, Magnetic properties of the iron-group metal phosphides. *J. Appl. Phys.* **38**, 1253–1255 (1967).

90. J. Gattacceca, P. Rochette, F. Lagroix, P.-E. Mathé, B. Zanda, Low temperature magnetic transition of chromite in ordinary chondrites. *Geophys. Res. Lett.* **38**, L10203 (2011).

91. J. L. Carter, VLS (Vapor-Liquid-Solid): Newly discovered growth mechanism on the lunar surface? *Science* **181**, 841–842 (1973).

92. I. McDougall, T. M. Harrison, *Geochronology and Thermochronology by the 40Ar/39Ar Method* (Oxford Univ. Press, ed. 2, 1999).

93. O. Eugster, G. F. Herzog, K. Marti, M. W. Caffee, in *Meteorites and the Early Solar System II*, D. S. Lauretta, H. Y. McSween, Eds. (University of Arizona Press, 2006), pp. 829–851.

94. O. Eugster, D. Terriblini, E. Polnau, J. Kramers, The antiquity indicator argon-40/argon-36 for lunar surface samples calibrated by uranium-235-xenon-136 dating. *Meteorit. Planet. Sci.* **36**, 1097–1115 (2001).

95. K. H. Joy, D. A. Kring, D. D. Bogard, D. S. McKay, M. Zolensky, Re-examination of the formation ages of the Apollo 16 regolith breccias. *Geochim. Cosmochim. Acta* **75**, 7208–7225 (2011).

96. D. Stöffler, G. Ryder, B. A. Ivanov, N. A. Artemieva, Cratering history and lunar chronology. *Rev. Mineral. Geochem.* **60**, 519–596 (2006).

97. L. Husain, in *The Apollo 15 Lunar Samples* (Lunar and Planetary Institute, 1972), pp. 374–375.

98. R. W. Carlson, G. W. Lugmair, Sm-Nd constraints on early lunar differentiation and the evolution of KREEP. *Earth Planet. Sci. Lett.* **45**, 123–132 (1979).

99. P. Vermeesch, IsoplotR: A free and open toolbox for geochronology. *Geosci. Front.* **9**, 1479–1493 (2018).

100. H. H. Schmitt, N. E. Petro, R. A. Wells, M. S. Robinson, B. P. Weiss, C. M. Mercer, Revisiting the field geology of Taurus-Littrow. *Icarus* **298**, 2–33 (2017).

101. R. D. Warner, G. F. Taylor, G. H. Conrad, H. R. Northrop, S. Barker, K. Keil, Apollo 17 high-Ti mare basalts: New bulk compositional data, magma types, and petrogenesis. *Proc. Lunar Planet Sci. Conf. 10th* **1**, 225–247 (1979).

102. J. B. Paces, S. Nakai, C. R. Neal, L. A. Taylor, A. N. Halliday, D.-C. Lee, A strontium and neodymium isotopic study of Apollo 17 high-Ti mare basalts: Resolution of ages, evolution of magmas, and origins of source heterogeneities. *Geochim. Cosmochim. Acta* **55**, 2025–2043 (1991).

103. D. Phinney, S. B. Kahl, J. H. Reynolds, 40Ar/39 Ar dating of Apollo 16 and 17 rocks. *Proc. Lunar Sci. Conf. 6th* **2**, 1593–1608 (1975).

Citation: S. Mighani, H. Wang, D. L. Shuster, C. S. Borlina, C. I. O. Nichols, B. P. Weiss, The end of the lunar dynamo. *Sci. Adv.* **6**, eaax0883 (2020).